

Pulsating active matter

Yiwei Zhang and Étienne Fodor

Department of Physics and Materials Science, University of Luxembourg, L-1511 Luxembourg, Luxembourg

Cells in tissues consume fuel to sustain periodic mechanical deformation. The combination of individual deformation and local interactions yields contraction waves, propagating throughout tissues with only negligible cell displacement. We consider a model of dense repulsive particles whose activity drives periodic change in size of each individual. It reveals that, in dense environments, pulsation of synchronised particles is a generic route to contraction waves. The competition between repulsion and synchronisation triggers an instability which promotes a wealth of dynamical patterns, ranging from spiral waves to defect turbulence. We identify the mechanisms underlying the emergence of patterns, and characterize the corresponding transitions. We derive the hydrodynamics of our model, and propose an analogy with that of reaction-diffusion systems.

Active matter features injection of energy at individual level to sustain nonequilibrium dynamics [1–3]. The interplay between particle interaction and individual activity opens the door to collective behaviours without any equilibrium counterpart. In many studies, activity takes the form of self-propulsion: Each particle converts the energy provided by some fuel into translational motion. Depending on microscopic symmetries, self-propelled particles can exhibit flocking transition [4] and/or motility-induced phase separation [5], for instance. In dense regimes, self-propulsion shifts the glass transition [6, 7]. It also controls the solid-fluid transition in models of cellular tissues, where the area and perimeter of each cell are constrained by interactions [8, 9].

Activity is not restricted to self-propulsion in general. In biological tissues, living cells use chemical energy to undergo mechanical deformation. For instance, collectively increasing and decreasing their size in a periodic and synchronised fashion [10]. To maintain close packing, local increase in density induces nearby decrease: Tissues must accommodate coexistence between contracting and expanding regions. This promotes propagation of contraction waves and pulses, as reported both *in vivo* [11–13] and *in vitro* [10, 14–19].

The emergence of collective contraction is of tremendous importance in many biological contexts. During morphogenesis, mechanochemical coupling yields wave propagation driving the early stages of embryonic development [20–22]. In cardiac tissue, electromechanical coupling leads to contraction pulses spontaneously organizing in patterns [23–25], some of which signal arrhythmogenesis [26, 27]. In uterine tissue, a similar coupling regulates large-scale contraction during labor [28, 29]. For all cases, understanding how to control contractile patterns is a first step towards mitigating various health issues.

Some models, from particles [16, 30] to hydrodynamics [31, 32], capture contraction waves by regarding activity as a combination of self-propulsion and contraction. Yet, it can be surprising to regard translational motion as the dominant nonequilibrium factor when cells barely move. Indeed, even when biological tissues behave as solids, collective states supported by individual

deformation can still emerge. Some preliminary works have considered models where activity sustains size oscillations [33–37], which indeed leads to novel Physics compared with that of self-propelled particles. Here, we formulate a model of pulsating active matter (PAM) which reveals that individual pulsation is indeed key to a wealth of dynamical phenomena [Fig. 1][38].

Model.—We consider N deforming particles in two dimensions subject to the pair-wise repulsive potential U . The overdamped dynamics of positions $\{\mathbf{r}_i\}$ reads

$$\dot{\mathbf{r}}_i = -\mu \sum_j \partial_{\mathbf{r}_i} U(a_{ij}) + \sqrt{2D} \boldsymbol{\xi}_i, \quad a_{ij} = \frac{|\mathbf{r}_i - \mathbf{r}_j|}{\sigma(\theta_i) + \sigma(\theta_j)}, \quad (1)$$

where μ and D are respectively the mobility and diffusivity, and $\boldsymbol{\xi}_i$ is an isotropic Gaussian white noise with zero mean. We take $U(a) = U_0(a^{-12} - 2a^{-6})$ for $a < 1$, and $U(a) = 0$ otherwise. The interaction range is controlled by the particle size $\sigma(\theta_i)$ given by

$$\sigma(\theta_i) = \sigma_0 \frac{1 + \lambda \sin \theta_i}{1 + \lambda}, \quad (2)$$

where σ_0 is the largest size, and $\lambda < 1$. We regard the

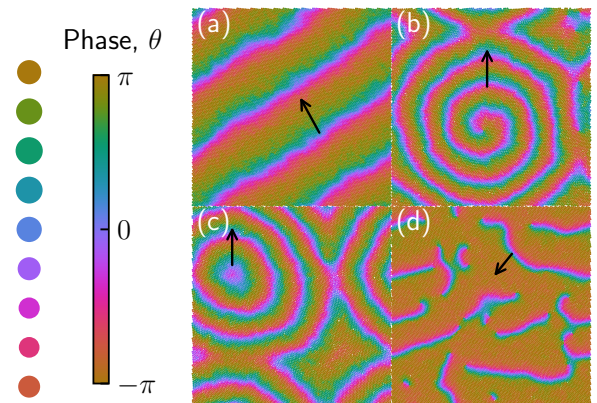


FIG. 1. Repulsive particles with pulsating size yield contraction waves: (a) planar, (b) spiral, (c) circular, and (d) turbulent. Waves propagation (black arrows) stabilizes dynamical patterns reminiscent of reaction-diffusion systems [38].

phases $\{\theta_i\}$ as stochastic degrees of freedom subject to the drive ω , which sustains periodic deformation of particles, and to the local synchronisation \mathcal{T} :

$$\dot{\theta}_i = \omega - \sum_j \left[\mathcal{T}(a_{ij}, \theta_i - \theta_j) + \mu_\theta \partial_{\theta_i} U(a_{ij}) \right] + \sqrt{2D_\theta} \eta_i, \quad (3)$$

where μ_θ and D_θ are the effective mobility and diffusivity of phases, and η_i is a Gaussian white noise with zero mean. The synchronisation range is the same as that of repulsion: $\mathcal{T}(a, \theta) = \varepsilon \sin(\theta)$ for $a < 1$, and $\mathcal{T}(a, \theta) = 0$ otherwise. Our dynamics reduces to a set of passive deforming particles when $\omega = 0$ and $\mathcal{T} = 0$ [39, 40].

Patterns and phases.—The repulsion terms $\partial_{\mathbf{r}_i} U$ and $\partial_{\theta_i} U$ minimize particle overlap, which promotes a uniform density profile, and impedes (facilitates) the expansion (contraction) of particles whenever they are in contact. In contrast with previous works on driven deforming particles [33, 34], the packing fraction φ here varies in time when particle sizes $\sigma(\theta_i)$ are cycling:

$$\varphi = \pi \sum_{i=1}^N (\sigma(\theta_i)/L)^2, \quad (4)$$

where L is the system size. Above a given density, repulsion precludes that all particles simultaneously reach their largest size. Yet, synchronisation puts a cost on phase differences between neighbours, thus favoring a uniform phase profile. The competition between repulsion and synchronisation can then destabilize the uniform phase profile, yielding contraction waves, while the density profile stays roughly homogeneous. It leads to dynamical patterns which are either steady, taking the form of planar, spiral, or circular waves [Figs. 1(a-c)], or continuously changing [Figs. 1(d)]. Besides, some patterns are associated with defects in the phase profile [Figs. 1(b-d)]. Overall, our minimal model entails a phenomenology reminiscent of reaction-diffusion systems (RDS) [41, 42], where waves propagate with only negligible particle displacement. In contrast with RDS, the instability underlying pattern formation does not rely here on any chemical reaction, it only stems from mechanical deformation and synchronisation.

We characterize the emergent phenomenology in terms of the phase dynamics, given that the signature of patterns in the position dynamics is less straightforward. The uniform phase profile is a fully synchronized state, with most particles sharing the same phase at each time, whereas contraction waves and defects accommodate phase inhomogeneities. In that respect, we regard the emergence of waves as a transition from order to disorder in terms of the synchronisation parameter

$$r = \frac{1}{N} \left| \sum_{j=1}^N e^{i\theta_j} \right|. \quad (5)$$

Varying the total density ρ_0 and the synchronisation strength ε , which regulate the repulsion-synchronisation trade-off, we observe two disconnected regions where the averaged parameter $\langle r \rangle$ is close to unity [Fig. 2(a)]. The ordered state is cycling at small density ($\rho_0 < 1.5$) and arrested at large density ($\rho_0 > 1.8$). Waves emerge in between these states (large ε and moderate ρ_0) through a transition destabilizing either the cycling or the arrested ordered state, yielding $\langle r \rangle$ smaller than unity. We regard waves as a locally ordered, yet globally disordered state, at variance with disorder at smaller ε where the system is both locally *and* globally disordered.

Overall, we delineate three boundaries in the phase diagram [43][Fig. 2(a)]: (i) at small density ($\rho_0 < \rho_c$, $\rho_c \approx 1.3$), $\varepsilon_{b,1}(\rho_0)$ decreases with ρ_0 [dark green line], (ii) at moderate density ($\rho_c < \rho_0 < 1.5$), $\varepsilon_{b,2}(\rho_0)$ increases with ρ_0 [dark red line], and (iii) at high density ($\rho_0 > 1.8$), $\varepsilon_{b,3}(\rho_0)$ merely depends on ε [dark blue line]. In what follows, we analyze the nature of these transitions, identify the corresponding microscopic mechanisms, and construct a hydrodynamic description of PAM revealing an analogy with RDS.

Ordered states: Cycling and arrest.—At small density ($\rho_0 < \rho_c$), particles barely overlap, so that the effect of repulsion in Eq. (3) is subdominant compared with synchronisation. Our setting is then akin to the seminal Kuramoto model [44], albeit neighbour identities now vary

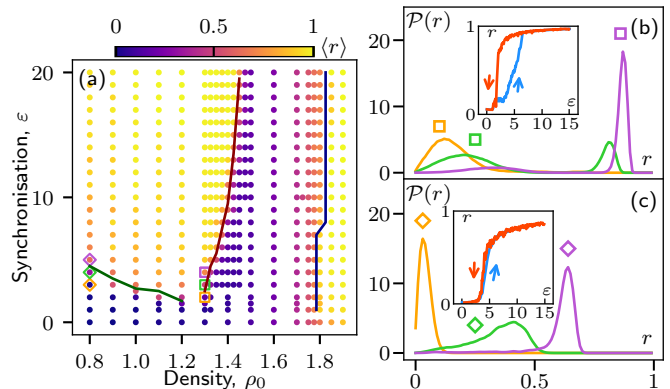


FIG. 2. Phases and transitions in particle-based dynamics. (a) We distinguish two ordered states ($\langle r \rangle \approx 1$) where particles are either cycling in phase (small ρ_0 and large ε) or arrested (large ρ_0). The solid lines in dark green ($\varepsilon_{b,1}(\rho_0)$), dark red ($\varepsilon_{b,2}(\rho_0)$), and dark blue ($\varepsilon_{b,3}(\rho_0)$) are guidelines delineating the boundaries between ordered and disordered states [43]. Dynamical patterns and waves [Fig. 1] emerge in the disordered state at large ε , in between the phase boundaries $\varepsilon_{b,2}(\rho_0)$ and $\varepsilon_{b,3}(\rho_0)$. (b) At $\rho_0 = 1.3$, the distribution $\mathcal{P}(r)$ changes between unimodal and bimodal shapes when varying ε through the phase boundary $\varepsilon_{b,2}(\rho_0)$ [squares in (a)]. The transition is discontinuous with hysteresis [inset]. (c) At $\rho_0 = 0.8$, $\mathcal{P}(r)$ stays unimodal through the boundary $\varepsilon_{b,1}(\rho_0)$ [diamonds in (a)]. The transition is continuous without hysteresis [inset].

in time. Given that all phases are driven at the same frequency, the system orders whenever the synchronisation overcomes the noise. At mean-field level, this requires $\rho_0 \varepsilon$ greater than a factor proportional to D_θ , which is consistent with $\varepsilon_{b,1}(\rho_0)$ decreasing with ρ_0 .

At high density ($\rho_0 > 1.8$), particles are too packed to cycle their phase. The ordered state is arrested, with particle sizes fluctuating around an average value given by close packing, without any phase current. To build intuition on how arrest emerges, we approximate the repulsive term in Eq. (3) as $\partial_{\theta_i} U = (\partial_\varphi U)(\partial_{\theta_i} \varphi)$, with $\partial_\varphi U$ independent of $\{\theta_i\}$ to first approximation. Hence, we map the pairwise potential U into the effective one-body potential $U_{\text{eff}} = (\partial_\varphi U) \varphi$, which is a periodic function of each phase θ_i . The drive tilts this potential as $U_{\text{eff}} - \omega \sum_i \theta_i$. At small ω (equivalently, large $\partial_\varphi U$), phases are trapped in a local minimum of the tilted potential, yielding arrest. In this regime, the potential contribution is overwhelmingly dominant compared with synchronisation, so that $\varepsilon_{b,3}(\rho_0)$ weakly depends on ε .

Beyond ordered states: Waves and defects.—Reducing ρ_0 decreases $\partial_\varphi U$, which lowers the depth of local minima in the tilted potential. Fluctuations can then trigger jumps between minima, which promotes transient cycling of size. As a result, the system now features spatial coexistence between cycling and arrested particles, which yields $\langle r \rangle$ smaller than 1, and destabilizes the homogeneous phase profile. At large ε , the synchronisation leads local cycling to propagate between nearest neighbours, yielding contraction waves in an arrested background [Fig. 1(d)]. Interestingly, defects are present at both ends of each wave, rotating in opposite directions [38]. Such defect pairs spontaneously form, move, and annihilate, thus forming a dynamical state analogous to the defect turbulence reported in RDS [45].

As ρ_0 gets smaller, more particles are prone to cycling, which reduces the proportion of arrested particles, and yields smaller $\langle r \rangle$. For $\langle r \rangle$ close to 0, namely when all particles cycle, dynamical patterns spontaneously organize into specific structures: Either planar, spiral, or circular waves [Figs. 1(a-c)]. Correspondingly, we observe that the number of defects is much reduced, and defects are also less motile than in defect turbulence. Eventually, further decreasing ρ_0 , the system enters the cycling ordered state [top left of Fig. 2(a)].

We now examine how the distribution $\mathcal{P}(r)$ varies through the phase boundaries $\varepsilon_{b,1}(\rho_0)$ and $\varepsilon_{b,2}(\rho_0)$, which respectively decrease and increase with ρ_0 . For the boundary $\varepsilon_{b,2}(\rho_0)$, \mathcal{P} is peaked at small r in the disordered state, and it becomes bimodal as the system orders, with weight shifting from small to large r [Fig. 2(b)]. This indicates the existence of a metastable regime where both states are linearly stable. Starting deep in the ordered state and reducing ε , a fluctuation eventually destabilizes the global synchronisation, and triggers a discontinuous transition towards small r [inset of Fig. 2(b)]. Conversely,

starting from the disordered state and increasing ε reveals hysteresis, another signature of metastability. A similar analysis for the boundary $\varepsilon_{b,1}(\rho_0)$ shows that \mathcal{P} now stays unimodal [Fig. 2(c)], the increase/decrease of r with ε appears continuous, and the hysteresis is weak [inset of Fig. 2(c)]. In other words, metastability progressively disappears when reducing ρ_0 , showing how repulsion changes the nature of the transition.

Current statistics.—Repulsion puts a strong constraint on phase dynamics whenever the packing fraction of large particles $\rho_0 \pi \sigma_0^2$ is comparable with close packing. In this regime, overlap between particles accelerates (decelerates) their contraction (expansion). As a result, the packing fraction φ oscillates in quadrature (phase shift of $\pi/2$ in natural units) with the scaled instantaneous phase velocity

$$\nu = \frac{1}{N\omega} \sum_{j=1}^N \dot{\theta}_j. \quad (6)$$

In the cycling ordered state, strong repulsion yields oscillations with high amplitude [Fig. 3(a)]. In the disordered state with patterns, phase shift between neighbours enables a smaller overlap and a reduced oscillation amplitude [Fig. 3(b)]. We detect the corresponding transition in terms of the current variance $\text{Var}(\nu) = \langle \nu^2 \rangle - \langle \nu \rangle^2$ [Fig. 3(c)]. In the ordered state, $\text{Var}(\nu)$ increases steadily with ρ_0 until it abruptly drops. The location of this drop is close to the boundary $\varepsilon_{b,2}(\rho_0)$ [Fig. 2(a)].

The averaged parameter $\langle \nu \rangle$ is close to 1 throughout the phase diagram, except in the arrested ordered state ($\rho_0 > 1.8$) where ν vanishes [43]. In that respect, contraction waves can be regarded as the collective strategy which, by introducing local phase shifts, enables to maintain high $\langle \nu \rangle$ even at high ρ_0 . Importantly, synchronisation mitigates high phase shift, promoting bands

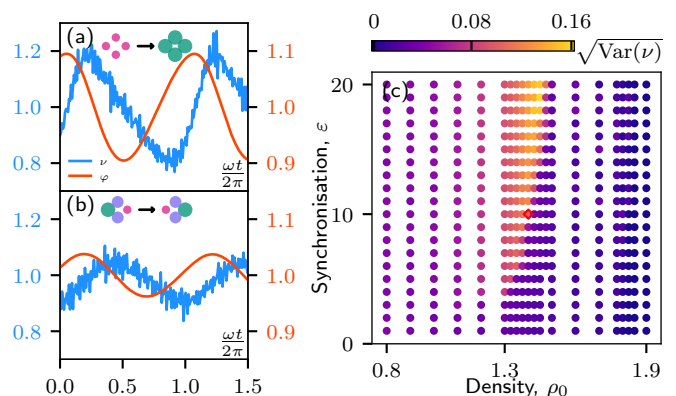


FIG. 3. Packing fraction φ and current ν oscillate in quadrature, with higher amplitude for (a) globally synchronized particles than for (b) dynamical patterns. Trajectories in (a) and (b) are sampled for the same (ε, ρ_0) [diamond in (c)]. (c) The current variance $\text{Var}(\nu)$ changes abruptly close to the phase boundary $\varepsilon_{b,2}(\rho_0)$ [same line as in Fig. 2(a)].

with equal phase. Therefore, in contrast with previous works [33, 34], synchronisation here stands out as the essential ingredient for stabilizing patterns. In short, the transition at $\varepsilon_{b,2}(\rho_0)$ arises from a competition favoring either synchronisation at the cost of overlap, or smaller overlap at the cost of reduced synchronisation.

Hydrodynamics.—The contraction waves in Figs. 1(a-d) are reminiscent of the chemical waves in RDS [41, 42]. Although the microscopic details of PAM and RDS are quite different, it is tempting to draw analogies between their hydrodynamics. For simplicity, setting $\mu = 0$, we neglect the role of repulsion in density fluctuations. In the phase dynamics, we assume that the interaction range is perfectly local: $\sum_j \mathcal{T}(a_{ij}, \theta_i - \theta_j) \approx \pi \sigma_0^2 \varepsilon \sum_j \sin(\theta_i - \theta_j) \delta(\mathbf{r}_i - \mathbf{r}_j)$, and we treat repulsion as $\sum_j \partial_{\theta_i} U(a_{ij}) \approx \pi \sigma_0^2 (\partial_{\varphi} U) \sum_j (\partial_{\theta_j} \varphi) \delta(\mathbf{r}_i - \mathbf{r}_j)$, where $\partial_{\varphi} U$ is again assumed constant. Using coarse-graining procedures [43], we obtain a closed dynamics for the local order parameter $A(\mathbf{r}, t) = \sum_j e^{i\theta_j} \delta(\mathbf{r} - \mathbf{r}_j(t))$ in powers of A and its gradients:

$$\begin{aligned} \partial_t A = & \left(\frac{\bar{\varepsilon} \rho_0}{2} - D_{\theta} + i\omega + D\nabla^2 \right) A - \frac{\bar{\varepsilon}^2 A |A|^2}{4(2D_{\theta} - i\omega)} \\ & - icA \left[\text{Re}(A) + \frac{\bar{\varepsilon} \lambda}{4} \text{Im} \left(\frac{A^2}{2D_{\theta} - i\omega} \right) \right] + \sqrt{\rho_0} D_{\theta} \Lambda, \end{aligned} \quad (7)$$

where $\bar{\varepsilon} = \pi \sigma_0^2 \varepsilon$, and $c = \mu_{\theta} \lambda (\pi \sigma_0 \sigma(0)/L)^2 (\partial_{\varphi} U)$. The field Λ is a Gaussian white noise with zero mean. This hydrodynamics is analogous to the complex Ginzburg-Landau equation describing a large class of RDS [46]. The term proportional to c in Eq. (7), which stems from the repulsive term $\partial_{\theta_i} U$ in Eq. (3), here breaks the gauge invariance $A \rightarrow A e^{i\Phi}$ for any Φ . This reveals how the coupling between repulsion and change in size at microscopic level affects the gauge symmetry of the hydrodynamic phase. Indeed, changing uniformly the phases of all particles does not leave the dynamics invariant due to particle overlap.

In the noiseless dynamics, the homogeneous profile is always linearly stable. It can correspond to order $|A| > 0$ or disorder $|A| = 0$. The former can be either arrested or cycling, respectively for constant and time-dependent ψ , where $A = |A| e^{i\psi}$. We obtain analytically the phase boundaries between these states [Fig. 4(a)]. The order-disorder transition follows $\bar{\varepsilon} \rho_0 = 2D_{\theta}$, in line with mean-field arguments for the particle-based dynamics. The term proportional to c in Eq. (7) controls the existence of stationary solutions for ψ . This highlights how microscopic repulsion induces arrest in hydrodynamics. At high density, repulsion gets rapidly enhanced with ρ_0 , so we take $c \propto \rho_0^n$ for $n > 0$. The arrested state then arises at large ρ_0 , and cycling occurs for intermediate density regimes between disorder and arrest, as expected. In short, our hydrodynamics reproduces the phase boundaries of the homogeneous states observed for particles [Fig. 2(a)].

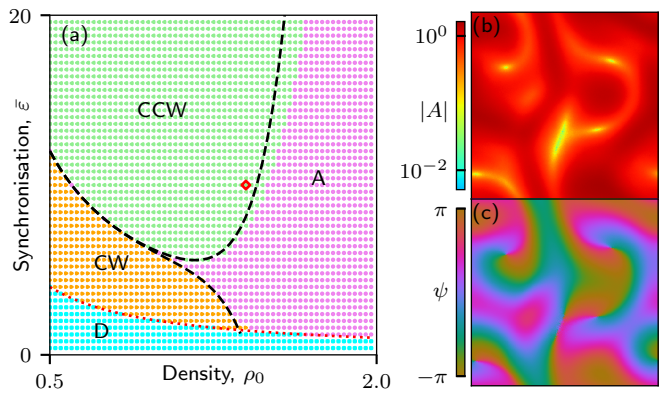


FIG. 4. (a) Phase diagram of homogeneous states in noiseless hydrodynamics: (D) disorder, (A) arrest, (CW) clockwise, and (CCW) counter-clockwise cycles. The red dotted line delineates order-disorder transition. The black dashed lines approximate the stability of arrest [43]. (b-c) In the presence of noise, steady states with motile defects appear for $(\bar{\varepsilon}, \rho_0)$ between cycling and arrest [diamond in (a)].

Due to non-linearities, homogeneous profiles are not the only stable solutions. In the presence of noise, between cycling and arrested states, the hydrodynamics now systematically reaches steady states with dynamical patterns [Figs. 4(b-c)]. They are always associated with motile defects constantly forming and merging, reminiscent of defect turbulence [Fig. 1(d)]. Interestingly, we do not observe waves with non-motile defects in contrast with microscopic simulations, suggesting that density fluctuations, neglected in our hydrodynamics, play an important role in stabilizing such structures.

Discussion.—It is striking that PAM entails hydrodynamic patterns akin to RDS. Indeed, our model does not feature any reaction, and particle diffusion is strongly hampered in dense regimes of interest. Yet, it is insightful to regard individual pulsation as a chemical reaction, whose coordinate is the particle phase, with ω effectively driving cycles between isomers. Importantly, this drive is a monomolecular reaction. Consistently, hydrodynamic non-linearities all stem from particle interactions: Setting $\bar{\varepsilon} = 0 = c$ yields a linear dynamics for A . The interplay between synchronisation, repulsion and deformation is then akin to mechano-chemical coupling, which indeed regulates cell size in tissues [47, 48].

Overall, our results show that cells do not need to self-propel to promote contractile patterns. This scenario should be robust when considering more complex interactions. Indeed, if the reference area and perimeter of deforming cells [8, 9] are pulsating, oscillations between elongated and rounded cells is again a route to wave propagation, given local synchronisation of cycling. Interestingly, our model reveals how density controls the crossover between wave types. In cardiac tissues, the emergence of spiral waves and turbulence signals fibrillation. Various strategies have been proposed to mitigate

this while avoiding drastic measures [26, 49, 50]. To this end, our model stands out as an appropriate platform in search of protocols inhibiting specific waves with local perturbation. Moreover, even for dense systems of macroscopic pulsating units, such as human crowds [51], it should still be relevant to delineate strategies which avoid disastrous contraction waves.

We acknowledge insightful discussions with Michael E. Cates, Luke K. Davis, Massimiliano Esposito, Robert L. Jack, Alessandro Manacorda, Xia-Qing Shi, Benjamin D. Simons, Julien Tailleur, and Frédéric van Wijland. Work funded by the Luxembourg National Research Fund (FNR), grant reference 14389168.

-
- [1] M. C. Marchetti, J. F. Joanny, S. Ramaswamy, T. B. Liverpool, J. Prost, M. Rao, and R. A. Simha, Hydrodynamics of soft active matter, *Rev. Mod. Phys.* **85**, 1143 (2013).
- [2] J. O’Byrne, Y. Kafri, J. Tailleur, and F. van Wijland, Time irreversibility in active matter, from micro to macro, *Nat. Rev. Phys.* **4**, 167 (2022).
- [3] E. Fodor, R. L. Jack, and M. E. Cates, Irreversibility and biased ensembles in active matter: Insights from stochastic thermodynamics, *Annu. Rev. Condens. Matter Phys.* **13**, 215 (2022).
- [4] H. Chaté, Dry aligning dilute active matter, *Annu. Rev. Condens. Matter Phys.* **11**, 189 (2020).
- [5] M. E. Cates and J. Tailleur, Motility-induced phase separation, *Annu. Rev. Condens. Matter Phys.* **6**, 219 (2015).
- [6] R. Ni, M. A. C. Stuart, and M. Dijkstra, Pushing the glass transition towards random close packing using self-propelled hard spheres, *Nat. Commun.* **4**, 2074 (2013).
- [7] L. Berthier, E. Flenner, and G. Szamel, Glassy dynamics in dense systems of active particles, *J. Chem. Phys.* **150**, 200901 (2019).
- [8] D. Bi, J. H. Lopez, J. M. Schwarz, and M. L. Manning, A density-independent rigidity transition in biological tissues, *Nat. Phys.* **11**, 1074 (2015).
- [9] D. Bi, X. Yang, M. C. Marchetti, and M. L. Manning, Motility-driven glass and jamming transitions in biological tissues, *Phys. Rev. X* **6**, 021011 (2016).
- [10] S. Zehnder, M. Suaris, M. Bellaire, and T. Angelini, Cell volume fluctuations in mdck monolayers, *Biophys. J.* **108**, 247 (2015).
- [11] A. C. Martin, M. Kaschube, and E. F. Wieschaus, Pulsed contractions of an actin – myosin network drive apical constriction, *Nature* **457**, 495 (2009).
- [12] J. Solon, A. Kaya-Copur, J. Colombelli, and D. Brunner, Pulsed Forces Timed by a Ratchet-like Mechanism Drive Directed Tissue Movement during Dorsal Closure, *Cell* **137**, 1331 (2009).
- [13] S. Armon, M. S. Bull, A. Aranda-Diaz, and M. Prakash, Ultrafast epithelial contractions provide insights into contraction speed limits and tissue integrity, *Proc. Natl. Acad. Sci. U.S.A.* **115**, E10333 (2018).
- [14] X. Serra-picamal, V. Conte, R. Vincent, E. Anon, D. T. Tambe, E. Bazellieres, J. P. Butler, J. J. Fredberg, and X. Trepat, Mechanical waves during tissue expansion, *Nat. Phys.* **8**, 628 (2012).
- [15] T. Sham, G. Estelle, L. Brigitte, C. Olivier, L. Benoît, D.-A. Hélène, and G. François, Collective cell migration without proliferation: density determines cell velocity and wave velocity, *R. Soc. Open Sci.* **5**, 172421 (2018).
- [16] V. Petrolli, M. Le Goff, M. Tadrous, K. Martens, C. Allier, O. Mandula, L. Hervé, S. Henkes, R. Sknepnek, T. Boudou, G. Cappello, and M. Balland, Confinement-induced transition between wavelike collective cell migration modes, *Phys. Rev. Lett.* **122**, 168101 (2019).
- [17] G. Peyret, R. Mueller, J. d’Alessandro, S. Begnaud, P. Marcq, R.-M. Mège, J. M. Yeomans, A. Doostmohammadi, and B. Ladoux, Sustained oscillations of epithelial cell sheets, *Biophys. J.* **117**, 464 (2019).
- [18] N. Hino, L. Rossetti, A. Marín-Llauradó, K. Aoki, X. Trepat, M. Matsuda, and T. Hirashima, Erk-mediated mechanochemical waves direct collective cell polarization, *Dev. Cell* **53**, 646 (2020).
- [19] D. Boockock, N. Hino, N. Ruzickova, T. Hirashima, and E. Hannezo, Theory of mechanochemical patterning and optimal migration in cell monolayers, *Nat. Phys.* **17**, 267 (2021).
- [20] C.-P. Heisenberg and Y. Bellaïche, Forces in tissue morphogenesis and patterning, *Cell* **153**, 948 (2013).
- [21] A. Bailles, C. Collinet, J.-M. Philippe, E. M. Pierre-François Lenne, and T. Lecuit, Genetic induction and mechanochemical propagation of a morphogenetic wave, *Nature* **572**, 467 (2019).
- [22] A. Bailles, E. W. Gehrels, and T. Lecuit, Mechanochemical principles of spatial and temporal patterns in cells and tissues, *Annu. Rev. Cell Dev. Biol.* **38**, null (2022).
- [23] A. Karma, Spiral breakup in model equations of action potential propagation in cardiac tissue, *Phys. Rev. Lett.* **71**, 1103 (1993).
- [24] J. Christoph, M. Chebbok, C. Richter, J. Schröder-Schetelig, P. Bittihn, S. Stein, I. Uzelac, F. H. Fenton, G. Hasenfuß, R. F. G. Jr., and S. Luther, Electromechanical vortex filaments during cardiac fibrillation, *Nature* **555**, 667 (2018).
- [25] A. Molavi Tabrizi, A. Mesgarnejad, M. Bazzi, S. Luther, J. Christoph, and A. Karma, Spatiotemporal organization of electromechanical phase singularities during high-frequency cardiac arrhythmias, *Phys. Rev. X* **12**, 021052 (2022).
- [26] A. Karma, Physics of cardiac arrhythmogenesis, *Annu. Rev. Condens. Matter Phys.* **4**, 313 (2013).
- [27] W.-J. Rappel, The physics of heart rhythm disorders, *Phys. Rep.* **978**, 1 (2022).
- [28] J. Xu, S. N. Menon, R. Singh, N. B. Garnier, S. Sinha, and A. Pumir, The role of cellular coupling in the spontaneous generation of electrical activity in uterine tissue, *PLOS ONE* **10**, e0118443 (2015).
- [29] K. M. Myers and D. Elad, Biomechanics of the human uterus, *WIREs Syst. Biol. Med.* **9**, e1388 (2017).
- [30] S. Armon, M. S. Bull, A. Moriel, H. Aharoni, and M. Prakash, Modeling epithelial tissues as active-elastic sheets reproduce contraction pulses and predict rip resistance, *Commun. Phys.* **4**, 216 (2021).
- [31] K. Dierkes, A. Sumi, J. Solon, and G. Salbreux, Spontaneous oscillations of elastic contractile materials with turnover, *Phys. Rev. Lett.* **113**, 148102 (2014).
- [32] S. Banerjee, K. J. C. Utuje, and M. C. Marchetti, Propagating stress waves during epithelial expansion, *Phys. Rev. Lett.* **114**, 228101 (2015).
- [33] E. Tjhung and T. Kawasaki, Excitation of vibrational

- soft modes in disordered systems using active oscillation, *Soft Matter* **13**, 111 (2017).
- [34] E. Tjhung and L. Berthier, Discontinuous fluidization transition in time-correlated assemblies of actively deforming particles, *Phys. Rev. E* **96**, 050601 (2017).
- [35] Y. Togashi, Modeling of nanomachine/micromachine crowds: Interplay between the internal state and surroundings, *J. Phys. Chem. B* **123**, 1481 (2019).
- [36] Y. Koyano, H. Kitahata, and A. S. Mikhailov, Diffusion in crowded colloids of particles cyclically changing their shapes, *EPL* **128**, 40003 (2019).
- [37] N. Oyama, T. Kawasaki, H. Mizuno, and A. Ikeda, Glassy dynamics of a model of bacterial cytoplasm with metabolic activities, *Phys. Rev. Research* **1**, 032038 (2019).
- [38] See movies of numerical simulations at [URL will be inserted by publisher] corresponding to snapshots shown in Fig. 1.
- [39] A. Ninarello, L. Berthier, and D. Coslovich, Models and algorithms for the next generation of glass transition studies, *Phys. Rev. X* **7**, 021039 (2017).
- [40] C. Brito, E. Lerner, and M. Wyart, Theory for swap acceleration near the glass and jamming transitions for continuously polydisperse particles, *Phys. Rev. X* **8**, 031050 (2018).
- [41] A. M. Turing, The chemical basis of morphogenesis, *Philos. Trans. R. Soc. B Biol. Sci.* **237**, 37 (1952).
- [42] S. Kondo and T. Miura, Reaction-diffusion model as a framework for understanding biological pattern formation, *Science* **329**, 1616 (2010).
- [43] See Supplemental Material at [URL will be inserted by publisher] for details on analytical derivations and numerical simulations, which includes Refs. [52, 53].
- [44] J. A. Acebrón, L. L. Bonilla, C. J. Pérez Vicente, F. Ritort, and R. Spigler, The kuramoto model: A simple paradigm for synchronization phenomena, *Rev. Mod. Phys.* **77**, 137 (2005).
- [45] Q. Ouyang and J.-M. Flesselles, Transition from spirals to defect turbulence driven by a convective instability, *Nature* **379**, 143 (1996).
- [46] I. S. Aranson and L. Kramer, The world of the complex ginzburg-landau equation, *Rev. Mod. Phys.* **74**, 99 (2002).
- [47] J. Howard, S. W. Grill, and J. S. Bois, Turing's next steps: the mechanochemical basis of morphogenesis, *Nat. Rev. Mol. Cell. Biol.* **12**, 392 (2011).
- [48] P. Recho, A. Hallou, and E. Hannezo, Theory of mechanochemical patterning in biphasic biological tissues, *Proc. Natl. Acad. Sci. U.S.A.* **116**, 5344 (2019).
- [49] S. Luther, F. H. Fenton, B. G. Kornreich, A. Squires, P. Bittihn, D. Hornung, M. Zabel, J. Flanders, A. Gladuli, L. Campoy, E. M. Cherry, G. Luther, G. Hasenfuss, V. I. Krinsky, A. Pumir, R. F. G. Jr, and E. Bodenschatz, Low-energy control of electrical turbulence in the heart, *Nature* **475**, 235 (2011).
- [50] N. DeTal, A. Kaboudian, and F. H. Fenton, Terminating spiral waves with a single designed stimulus: Teleportation as the mechanism for defibrillation, *Proc. Natl. Acad. Sci. U.S.A.* **119**, e2117568119 (2022).
- [51] N. Bain and D. Bartolo, Dynamic response and hydrodynamics of polarized crowds, *Science* **363**, 46 (2019).
- [52] D. S. Dean, Langevin equation for the density of a system of interacting Langevin processes, *J. Phys. A: Math. Gen.* **29**, 24 (1996).
- [53] L. B. Cai, H. Chaté, Y. Q. Ma, and X. Q. Shi, Dynamical subclasses of dry active nematics, *Phys. Rev. E* **99**, 10601 (2019).